Journal of Power Sources 187 (2009) 586–590

Contents lists available at ScienceDirect

Journal of Power Sources

journal homepage: www.elsevier.com/locate/jpowsour

Short communication

Structural characteristics and electrochemical performance of layered $Li[Mn_{0.5-x}Cr_{2x}Ni_{0.5-x}]O_2$ cathode materials

N.K. Karan[a], M. Balasubramanian[b,*,1], D.P. Abraham[c], M.M. Furczon[c], D.K. Pradhan[d], J.J. Saavedra-Arias[a], R. Thomas[a], R.S. Katiyar[a,**,2]

[a] Department of Physics and Institute for Functional Nanomaterials, University of Puerto Rico, PO Box 23343, San Juan, PR 00931, USA
[b] X-ray Science Division, Advanced Photon Source, Argonne National Laboratory, Argonne, IL 60439, USA
[c] Chemical Sciences and Engineering Division, Argonne National Laboratory, Argonne, IL 60439, USA
[d] Department of Physics and Meteorology, Indian Institute of Technology, Khargapur 721302, India

ARTICLE INFO

Article history:
Received 29 September 2008
Received in revised form 7 November 2008
Accepted 10 November 2008
Available online 24 November 2008

Keywords:
Li-ion battery
Cathode
Electrochemistry
X-ray absorption
Edge position

ABSTRACT

$Li[Mn_{0.5-x}Cr_{2x}Ni_{0.5-x}]O_2$ ($0<2x<0.2$) (Mn/Ni = 1) cathode materials have been synthesized by a solution method. X-ray diffraction patterns of the as-prepared materials were fitted based on a hexagonal unit cell (α-$NaFeO_2$ layer structure). The extent of Li/Ni intermixing decreased, and layering of the structure increased, with increasing Cr content. Electrochemical cycling of the oxides, at 30 °C in the 3–4.3 V range vs. Li/Li^+, showed that the first charge capacity increased with increasing Cr content. However, maximum discharge capacity (~143 mAh g^{-1}) was observed for $2x = 0.05$. X-ray absorption near edge spectroscopic (XANES) measurements on the K-edges of transition metals were carried out on pristine and delithiated oxides to elucidate the charge compensation mechanism during electrochemical charging. The XANES data revealed simultaneous oxidation of both Ni and Cr ions, whereas manganese remains as Mn^{4+} throughout, and does not participate in charge compensation during oxide delithiation.

1. Introduction

In recent years $LiMn_{0.5}Ni_{0.5}O_2$ has emerged as an alternative to $LiCoO_2$, the currently used cathode material in Li-ion batteries [1–4]. $LiMn_{0.5}Ni_{0.5}O_2$ has a layered structure, which is isostructural to $LiCoO_2$, and contains manganese and nickel as tetravalent and divalent cations, respectively [5–7]. Because Mn^{4+} cannot be oxidized any further, the redox activity in $LiMn_{0.5}Ni_{0.5}O_2$ takes place on the nickel center, and two redox couples (Ni^{2+}/Ni^{3+} and Ni^{3+}/Ni^{4+}) are believed to be involved during the electrochemical intercalation–deintercalation of lithium [5–7]. Partial substitution of nickel and manganese in $LiNi_{0.5}Mn_{0.5}O_2$ by cobalt has reduced the Li/Ni intermixing, and has produced improvements in the electrochemical and thermal stability properties [8–10]. One such compound, $LiNi_{1/3}Mn_{1/3}Co_{1/3}O_2$, has been investigated extensively and is a leading candidate for the cathode active material in lithium-ion batteries for transportation applications [11,12].

However, because Co is expensive, other elements to replace Ni and Mn in $LiNi_{0.5}Mn_{0.5}O_2$ are being investigated. Some researchers have totally substituted the Ni with Cr to form $Li_{1+x}Cr_yMn_{1-y}O_2$ compounds, which contain Cr^{3+} and Mn^{4+} in the as-prepared oxide powders [13–15]. Alternatively, partial substitution of both Ni and Mn by Cr can, in principle, increase the electrochemically active species content, and lower the Li/Ni intermixing while maintaining the overall structural integrity of the Li-stoichiometric oxide (by keeping Mn/Ni = 1).

In this article we describe the synthesis of layered $Li[Mn_{0.5-x}Cr_{2x}Ni_{0.5-x}]O_2$ ($0<2x<0.2$) (Mn/Ni = 1) by a cost effective solution route. These macroscopic compositions can also be envisioned as solid solutions of $[y](LiCrO_2)$ $[1-y](LiNi_{0.5}Mn_{0.5}O_2)$ ($0 \le y \le 0.2$). Note that if chromium exists in the 3+ state, the oxidation states of Ni and Mn will be maintained as 2+ and 4+, respectively, and the formation of deleterious Mn^{3+} in the pristine compounds will in principle be avoided. The electrochemical characterization of these oxides was conducted in coin cells with a lithium counter electrode. The oxide structures were examined by X-ray diffraction (XRD) and the redox behavior of the various electrochemically active species was studied by X-ray absorption near edge spectroscopy (XANES), which provides information on the electronic structure (oxidation states) and site symmetries [16,17]. Knowledge of the redox chemistry, and an understanding of structural changes during the electrochemical delithiation/lithiation

* Corresponding author. Tel.: +1 630 252 0593; fax: +1 630 252 0580.
** Corresponding author. Tel.: +1 787 751 4210; fax: +1 787 764 2571.
E-mail addresses: e-mail@aps.anl.gov (M. Balasubramanian), rkatiyar@uprrp.edu (R.S. Katiyar).
[1] Tel.: +1 630 252 0593; fax: +1 630 252 0580.
[2] Tel.: +1 787 751 4210; fax: +1 787 764 2571.

0378-7753/$ – see front matter © 2008 Elsevier B.V. All rights reserved.
doi:10.1016/j.jpowsour.2008.11.061

cycling, can serve as a guide for the design of novel high-capacity cathode materials.

2. Experimental

Lithium acetate (99%) [$LiOOCCH_3{\cdot}2H_2O$], manganese acetate (98%) [$Mn(CH_3COO)_2{\cdot}4H_2O$], nickel acetate (99%) [$Ni(CH_3COO)_2{\cdot}4H_2O$], and chromium nitrate (98.5%) [$Cr(NO_3)_3{\cdot}9H_2O$] (all from Alfa Aesar) were used as precursors for synthesizing $LiMn_{0.5-x}Cr_{2x}Ni_{0.5-x}O_2$ powders by a chemical solution route. The stoichiometric amounts of these salts were dissolved separately in deionized water and acetic acid (~1:1 vol) by continuous stirring at ~50 °C. An extra 3% lithium was added to compensate for the possible lithium loss during high temperature annealing. Later, all solutions were mixed together (~200 ml) and stirred continuously at ~80 °C for 4 h. The solution was then dried at ~200 °C and the resulting powder was fired at 450 °C for 4 h in air to decompose the organics. Finally, the powder was calcined at 950 °C for 15 h in air. The structure of the as-synthesized powders was determined by X-ray diffraction using CuK_α radiation (Siemens D5000). XRD data were collected in the 10–80° range (in θ–2θ scan) with 0.02 step size; the patterns were refined by Rietveld method using the Fullprof package to obtain lattice parameters of the oxides [18]. The diffraction angle was calibrated using quartz (Quartz probe; Bruker-AXS) as an external standard.

Electrode laminates from the oxide powders were prepared by coating a mixture of 84 wt% oxide, 8 wt% acetylene black, and 8 wt% PVdF binder on a 30-μm-thick Al foil. Electrochemical performance data on the electrodes were obtained in 2032-type coin cells (1.6-cm^2 electrode area) with a Li-metal counter electrode, Celgard 2400 separator and an electrolyte containing 1.2 M $LiPF_6$ in an ethylene carbonate:ethyl methyl carbonate (EC:EMC) (3:7 by wt.) solvent. The coin cells were assembled in a glovebox under an Ar-atmosphere. The cells were cycled between 3 and 4.3 V at 30 °C using a constant current density of 5 mA g^{-1}.

X-ray absorption spectroscopy experiments (XAS) were performed in the PNC-XOR bending magnet beamline (20-BM) of the Advanced Photon Source at Argonne. Measurements at the Mn, Ni and Cr K-edges were performed in the transmission mode using gas ionization chambers to monitor the incident and transmitted X-ray intensities. A pair of Si(1 1 1) crystals was used to monochromatize the radiation. A rhodium-coated X-ray mirror was used to suppress higher order harmonics. Energy calibration was carried out by using the first inflection point of the spectrum of the appropriate metal foil [19]. XAS data were obtained, on fresh electrodes (no electrolyte exposure) and on electrodes that were charged to ~145 mAh g^{-1}, at room temperature in a specially designed spectro-electrochemical cell [20] that allowed transmission of the X-ray beam. The XAS measurements were carried out after the cells were allowed to equilibrate and attain a stable open circuit voltage (OCV).

3. Results and discussion

3.1. X-ray diffraction (XRD)

XRD patterns of the as-prepared $LiMn_{0.5-x}Cr_{2x}Ni_{0.5-x}O_2$ ($2x = 0$, 0.05, 0.1, 0.2) powders are shown in Fig. 1. All major diffraction peaks were indexed based on a hexagonal unit cell (α-$NaFeO_2$ type structure) with space group $R\bar{3}m$. The additional features between 20° and 25° may arise from the ordering of the lithium and transition metal ions in the transition metal layers [21]. Peaks of a secondary (very minor) phase were also observed in the XRD data, often as shoulders to the main $R\bar{3}m$ peaks. The content of this phase decreased with increasing Cr concentration in the oxide powders. The identity of this secondary phase is uncertain at this time.

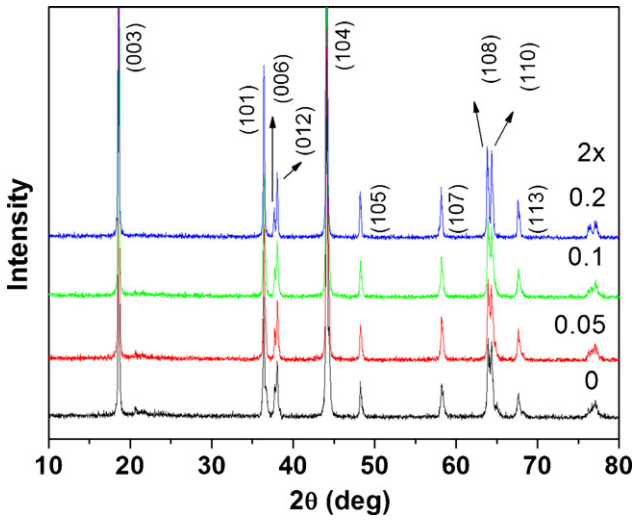

Fig. 1. XRD patterns of the as-prepared $LiMn_{0.5-x}Cr_{2x}Ni_{0.5-x}O_2$ cathode materials.

In the $R\bar{3}m$ structure, Li ions occupy 3b (0, 0, 0.5) sites, transition metal ions (Mn, Ni, Cr) occupy 3a (0, 0, 0) sites, and oxygen atoms occupy the 6c (0, 0, z) sites. In $LiMn_{0.5}Ni_{0.5}O_2$, Ni is in 2+ oxidation state and the ionic radius of Ni^{2+} (0.69 Å) is similar to that of Li^+ (0.76 Å). Therefore, a partial exchange of occupancy of Li and transition metal ions (mainly nickel) among the sites gives rise to cation mixing. For our refinements we varied several parameters that included the oxygen atom location (z value, Z_O) and the degree of cation mixing. For $LiMn_{0.5}Ni_{0.5}O_2$ ($2x = 0$ composition), the best fits were obtained for Li and Ni ion exchange between 3a and 3b sites of about 0.13 at. fraction for the sample with $2x = 0.0$ composition, which is comparable to reported values [22]. The extent of Li and Ni intermixing decreased with increasing Cr content. The lattice parameters obtained from the best fits are given in Table 1. The c and c/a values increase with increasing Cr content in the oxide. Furthermore, the (0 0 3)/(1 0 4) peak intensity ratios increase indicating that the oxide structure becomes more layered with increasing Cr content.

3.2. Electrochemistry

The first cycle charge–discharge profiles of the oxide electrodes obtained at 30 °C are shown in Fig. 2; capacity and electrochemistry efficiency (ratio of the discharge to charge capacity) values are given in Table 1. It is evident that the charge capacity increases with increasing Cr content. However, the discharge capacity does not show the same trend; the maximum discharge

Table 1
Rietveld refined structural parameters and electrochemical characteristics of the $LiMn_{0.5-x}Cr_{2x}Ni_{0.5-x}O_2$ cathodes.

$2x$	a (Å)	c (Å)	c/a	I_{003}/I_{104}	Z_O	Charge capacity (mAh g^{-1})	Discharge capacity (mAh g^{-1})	Coulombic efficiency (%)
0.0	2.8950(2)	14.303(1)	4.941	1.34	0.2563(2)	150.3	130.8	87.1
0.05	2.8946(2)	14.309(1)	4.943	1.49	0.2565(2)	164.9	143.1	86.7
0.1	2.8950(2)	14.321(1)	4.947	1.52	0.2561(2)	168.8	135.7	80.4
0.2	2.8934(2)	14.337(1)	4.955	1.58	0.2564(1)	174.6	124.3	71.12

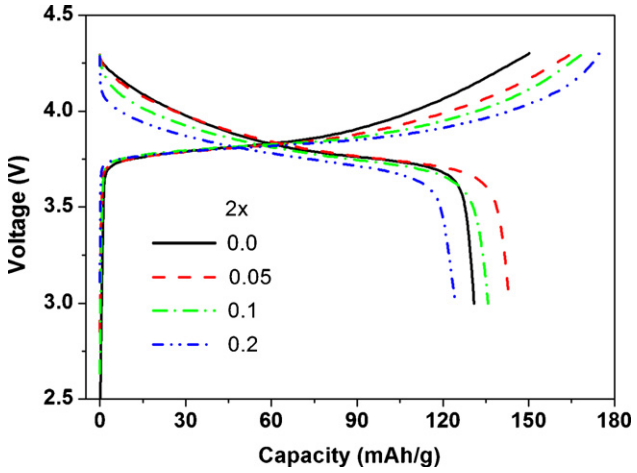

Fig. 2. First cycle charge–discharge profiles of $LiMn_{0.5-x}Cr_{2x}Ni_{0.5-x}O_2$ cathode materials at 30 °C in the voltage range 3–4.3 V using a constant current density of 5 mA g^{-1}.

capacity, 143 mAh g^{-1}, is observed for the $2x = 0.05$ composition. The discharge capacity decreases at higher Cr contents, with the smallest capacity observed for the $2x = 0.2$ composition. It is apparent that the discharge capacity trend does not correlate with the increased oxide layering observed at higher Cr contents. That is, the reduction of Ni content in the Li layer does not increase discharge capacity.

Table 1 shows that the electrochemistry efficiency decreases, i.e., the fraction of the extracted Li (during charging) that can be reinserted into the oxide structure during discharge decreases with increasing Cr content. The lower first cycle efficiencies at higher Cr contents could be due to diffusion limitations, which is typical for some layered phases [23,24]. Previous investigators have suggested that in layered $Li_{1.2}Cr_{0.4}Mn_{0.4}O_2$, Cr^{3+} oxidizes to Cr^{6+} during charge, which migrates to the vacant tetrahedral site from the original Cr^{3+} octahedral site [25]. The extraction/reinsertion of lithium in such materials is coupled with the migration of chromium, causing the process to be sluggish; i.e., compromised rate-capability that is associated with poor lithium diffusion kinetics.

3.3. X-ray absorption near edge spectroscopy (XANES)

Normalized Mn K-edge XANES spectra for as-prepared and delithiated $Li_{1-y}Mn_{0.5-x}Cr_{2x}Ni_{0.5-x}O_2$ electrodes are shown in Fig. 3(a) and (b), respectively. The Mn K-edge spectrum of as prepared $Li_{1.2}Cr_{0.4}Mn_{0.4}O_2$ is also shown for comparison. It is evident from Fig. 3(a) that the Mn K edge position and edge shape for all the as-prepared Cr-bearing oxides are very similar, and are comparable to the data from $Li_{1.2}Cr_{0.4}Mn_{0.4}O_2$ and $LiMn_{0.5}Ni_{0.5}O_2$, in which Mn is known to be in the 4+ oxidation state [5,15,25].

Changes in the spectra are observed on delithiation (Fig. 3(b)), which are, however, quite similar for all the $Li_{1-y}Mn_{0.5-x}Cr_{2x}Ni_{0.5-x}O_2$ compositions. When compared to the as-prepared oxide spectrum, the delithiated oxide spectra do not show a rigid shift in energy position to higher values, which indicates that manganese ions remain in the 4+ oxidation state during Li extraction. However, distinct changes in the edge shape in the delithiated oxide samples are observed, which probably result from a local rearrangement around the Mn ions in the oxide structure. Similar observations on Mn K-edge position and shape have been reported during delithiation of $Li_{1.2}Cr_{0.4}Mn_{0.4}O_2$ and $LiMn_{0.5}Ni_{0.5}O_2$ electrodes [5,15,25].

Normalized Cr K-edge spectra for as-prepared $LiMn_{0.5-x}Cr_{2x}Ni_{0.5-x}O_2$ electrodes are shown in Fig. 4(a). Data from as prepared $Li_{1.2}Cr_{0.4}Mn_{0.4}O_2$ and $LiCrO_2$, in which Cr is known to be in the

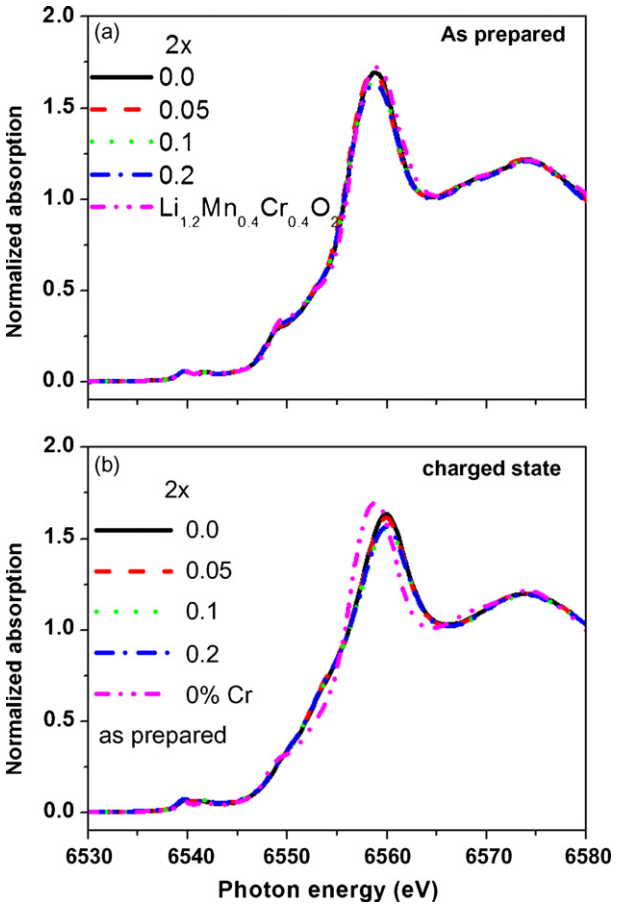

Fig. 3. Normalized Mn K-edge XANES spectra of (a) as-prepared and (b) electrochemically-delithiated $Li_{1-y}Mn_{0.5-x}Cr_{2x}Ni_{0.5-x}O_2$ cathodes. For comparison, as-prepared $Li_{1.2}Cr_{0.4}Mn_{0.4}O_2$ data is included in (a), and as-prepared sample spectrum for the ($2x = 0.00$) composition has been included in (b).

3+ oxidation state, are also included for comparison [15]. In general, the edge position and overall shape of the spectra for all $LiMn_{0.5-x}Cr_{2x}Ni_{0.5-x}O_2$ compositions are similar, and comparable to that for $LiCrO_2$, which indicates the presence of Cr^{3+} in the oxides. However, the pre-edge region of the $2x = 0.2$ composition is slightly different from those of the other compounds.

The details in the pre-edge region provide valuable information on the oxidation state of the Cr absorbers [25]. Chromium often occurs as Cr^{3+} or Cr^{6+} ions in its oxygen-based compounds. The Cr^{3+} ions tend to prefer octahedral coordination, whereas Cr^{6+} ions prefer tetrahedral coordination with oxygen. The XANES spectra of Cr^{6+} compounds exhibit a prominent pre-edge feature that is attributed to a bound $1s \rightarrow 3d$ transition [26,27]. This transition is forbidden in octahedral $Cr^{3+}O_6$ coordination, which has a center of inversion symmetry, but is allowed for non-centrosymmetric tetrahedral $Cr^{6+}O_4$ coordination due to the mixing of Cr(3d) with O(2p) orbitals. This mixing, in combination with the empty d-orbital ($3d^0$ configuration) of tetrahedral Cr^{6+} ions, increases the probability of the $1s \rightarrow 3d$ transition, resulting in many fold increase in the intensity of the pre-edge peak relative to octahedral Cr^{3+} [25]. The presence of a discernable pre-edge peak in Fig. 4(a) suggests that the $2x = 0.2$ oxide might contain a small amount (few percent) of Cr^{6+} along with Cr^{3+} ions in the as-prepared state.

On delithiation, the Cr K-edge edge position shifts rigidly to higher energies and the pre-edge peak intensity increases significantly (Fig. 4(b)). These observations indicate that on delithiation some of the Cr^{3+} ions are oxidized to Cr^{6+}. The intensity

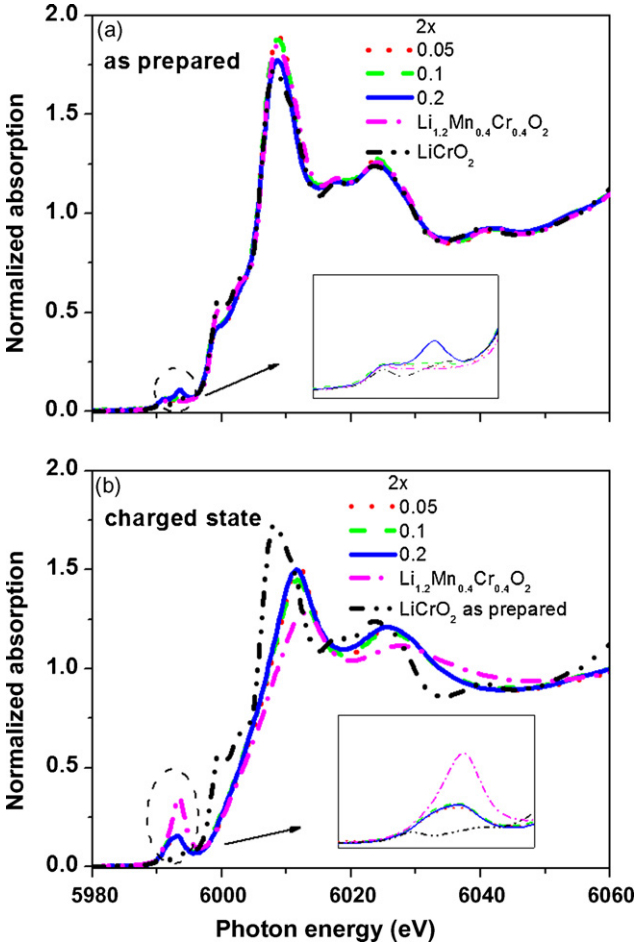

Fig. 4. Normalized Cr K-edge XANES spectra of (a) as-prepared and (b) electrochemically-delithiated $Li_{1-y}Mn_{0.5-x}Cr_{2x}Ni_{0.5-x}O_2$ cathodes. Data from as-prepared and electrochemically-delithiated $Li_{1.2}Cr_{0.4}Mn_{0.4}O_2$ samples are included for comparison. As-prepared $LiCrO_2$ sample spectrum is included in (b). Insets in both panels show an expanded view of the pre-edge region.

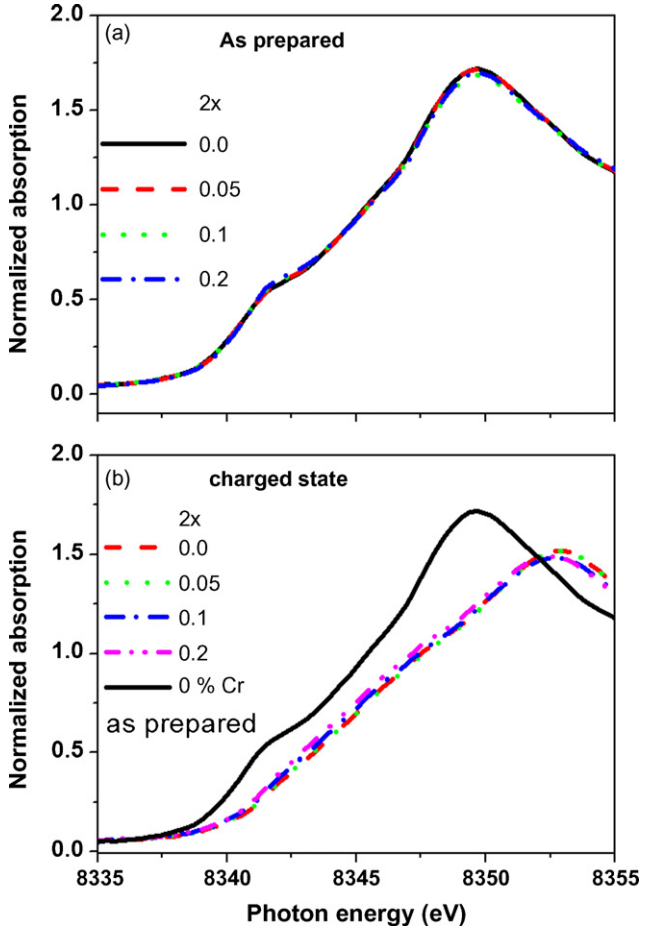

Fig. 5. Normalized Ni K-edge XANES spectra of (a) as-prepared, and (b) electrochemically-delithiated $Li_{1-y}Mn_{0.5-x}Cr_{2x}Ni_{0.5-x}O_2$ cathodes.

of the pre-edge peak appears to be similar for the various $Li_{1-y}Mn_{0.5-x}Cr_{2x}Ni_{0.5-x}O_2$ cathodes. However, in comparison to the Cr–Mn system (where the Mn is electrochemically inactive and all the charge compensation involves chromium ions [15,25]) the pre-edge intensity of $Li_{1-y}Mn_{0.5-x}Cr_{2x}Ni_{0.5-x}O_2$ is significantly smaller. Clearly, much lesser amount of tetrahedral Cr is present in these charged $Li_{1-y}Mn_{0.5-x}Cr_{2x}Ni_{0.5-x}O_2$ cells. Based on the pre-edge peak intensity and following the calibration curves reported by others, the amount of Cr^{6+} present at the charged state could be estimated [26,27]. The fraction of Cr^{6+} present at the charged state (~15% of the total Cr content) appears to be qualitatively independent of the oxide composition. Although the ratio of hexavalent chromium to total chromium is similar in all samples, we can infer that as the chromium content is increased the effective charge compensation delivered by the Cr^{3+}/Cr^{6+} couple increases. More specifically, for the $2x = 0.2$ sample, the Cr^{3+}/Cr^{6+} couple delivers four times more capacity when compared to the $2x = 0.05$ sample. As the cells were all charged to approximately the same capacity (~145 mAh g^{-1}), we expect that the charge compensation on the Ni will reduce as the chromium content is increased. This can be monitored by the Ni XANES measurements.

Normalized Ni K-edge XANES spectra for as-prepared $LiMn_{0.5-x}Cr_{2x}Ni_{0.5-x}O_2$ electrodes are shown in Fig. 5(a). The edge positions and shapes of Ni K XANES are similar for all $LiMn_{0.5-x}Cr_{2x}Ni_{0.5-x}O_2$ samples indicating that the oxidation state and local environment for the Ni are similar in all the as-prepared oxides. It is well established that in $LiMn_{0.5}Ni_{0.5}O_2$, Ni is predominately divalent [5,7]. On delithiation, the Ni K-edge in $Li_{1-y}Mn_{0.5-x}Cr_{2x}Ni_{0.5-x}O_2$ compounds shifts rigidly to higher energies (Fig. 5(b)), which indicates an increase in the average oxidation state of nickel. The shift decreases as the amount of chromium increases, suggesting a lower average oxidation state for Ni at the charged state with higher chromium content. This observation is consistent with the results of the Cr XANES. Previous studies have shown an ~1.5-eV shift in the position of the K-edge (measured at half step-height) per unit change in nickel oxidation state [16,28]. With respect to the starting cathode, the average oxidation state of nickel at the charged state can be estimated to increase by $\sim 1.45 \pm 0.07$, 1.49 ± 0.07, 1.23 ± 0.07 and 1.13 ± 0.07 for $2x = 0$, 0.05, 0.1 and 0.2, respectively.

Based on both Ni and Cr XANES results, we can infer that the charge compensation in these systems involves simultaneous participation of both nickel and chromium ions. This observations may be compared with data from the $LiNi_{0.85}Co_{0.15}O_2$ and $Li(Ni_{0.33}Co_{0.33}Mn_{0.33})O_2$ electrodes [16,29]. In both these systems, Ni ions oxidize during the initial stages of charge and attain a maximum oxidation state of Ni^{4+} well before the end of charge. Co ions, on the other hand, do not oxidize until 60–80% of lithium is extracted from the oxide during electrochemical charging. Some evidence for the participation of the oxygen sublattice in the charge compensation is also evident for $LiNi_{0.85}Co_{0.15}O_2$ and $Li(Ni_{0.33}Co_{0.33}Mn_{0.33})O_2$ electrodes. In sharp contrast, Ni^{2+} and Cr^{3+} oxidize simultaneously during delithiation of $LiMn_{0.5-x}Cr_{2x}Ni_{0.5-x}O_2$ compounds. Further

electrochemical and structural studies of $LiMn_{0.5-x}Cr_{2x}Ni_{0.5-x}O_2$ samples are currently underway and will be subsequently reported.

4. Summary

$LiMn_{0.5-x}Cr_{2x}Ni_{0.5-x}O_2$ ($2x = 0$, 0.05 0.1, 0.2) compounds were prepared by a chemical solution route. Major diffraction peaks from the as-prepared oxides could be indexed based on the $R\bar{3}m$ space group, which indicates that the oxides had well-defined layered structures. The lattice parameter and peak intensity data indicated that the extent of Li and Ni intermixing decreased with increasing Cr content in the oxide. XANES data showed that nickel, chromium and manganese are present predominantly in the divalent, trivalent and tetravalent state, respectively in the as-prepared samples. On electrochemical delithiation ($\sim$145 mAh g^{-1} capacity), charge compensation in the oxide structure is accomplished by the simultaneous oxidation of Ni^{2+} and Cr^{3+} ions, while the oxidation state of the manganese ions remained unchanged. Data from electrochemical cycling at 30 °C in the 3–4.3 V range vs. Li/Li^+ shows that oxide charge capacity increases with increasing Cr content. The discharge capacity, however, showed a maximum value for the $2x = 0.05$ oxide, and was lower for the $2x = 0.1$ and 0.2 compositions. These lower discharge capacities may be related to the presence of Cr^{6+} in the tetrahedral sites.

Acknowledgements

The financial support from DOE (DE-FGO2-01ER45868) and NASA-EPSCoR (NNX08AB12A) grant is gratefully acknowledged. One of us (N.K. Karan) is grateful to the NSF-EPSCoR for the graduate fellowship. Continual support from UPR Material Characterization Center (MCC) is also acknowledged. PNC/XOR is supported by the U.S. DOE, NSERC and its member institutions. The Advanced Photon Source is supported by the U.S.DOE, under contract DE-AC02-06CH11357. The CSE (Argonne) authors are grateful to Tien Duong and Dave Howell at the U.S. DOE, Office of Vehicle Technologies and to Gary Henriksen, ATD Program Manager at Argonne.

References

[1] T. Ohzuku, Y. Makimura, Chem. Lett. 30 (2001) 744.
[2] C.S. Johnson, J.-S. Kim, A.J. Kropf, A.J. Kahaian, J.T. Vaughey, L.M.L. Fransson, K. Edström, M.M. Thackeray, Chem. Mater. 15 (2003) 2313.
[3] S.-H. Kang, J. Kim, D. Abraham, M.E. Stoll, Y.-K. Sun, K. Amine, J. Power Sources 112 (2002) 41.
[4] K.M. Shaju, G.V. Subba Rao, B.V.R. Chowdari, Electrochim. Acta 48 (2003) 1505.
[5] W.-S. Yoon, C.P. Grey, M. Balasubramanian, X.-Q. Yang, J. McBreen, Chem. Mater. 15 (2003) 3161.
[6] J. Reed, G. Ceder, Electrochem. Solid-State Lett. 5 (2002) A145.
[7] A. Deb, U. Bergmann, S.P. Cramer, E.J. Cairns, J. Appl. Phys. 99 (2006) 063701.
[8] Z. Lu, D.D. McNeil, J.R. Dahn, Electrochem. Solid State Lett. 4 (2001) A200.
[9] B.C. Park, H.J. Bang, C.S. Yoon, S.T. Myung, J. Prakash, Y.K. Sun, J. Electrochem. Soc. 154 (2007) A520.
[10] J. Jiang, E.W. Ebrerman, L.J. Krause, J.R. Dahn, J. Electrochem. Soc. 152 (2005) A566.
[11] C.C. Chang, J.Y. Kim, P.N. Kumta, J. Electrochem. Soc. 149 (2002) A1114.
[12] Z. Chen, Y.K. Sun, K. Amine, J. Electrochem. Soc. 153 (2006) A1818.
[13] C. Storey, I. Kargina, Y. Grincourt, I.J. Davidson, Y. Yoo, D.Y. Seung, Proceedings of the 10th International Meeting on Lithium Batteries, Como, Italy, May 28–June 2, Abstract No. 234, 2000.
[14] Z. Lu, J.R. Dahn, J. Electrochem. Soc. 149 (2002) A1454.
[15] B. Ammundsen, J. Paulsen, I. Davidson, R.S. Liu, C.H. Shen, J.M. Chen, L.Y. Jang, J.F. Lee, J. Electrochem. Soc. 149 (2002) A431.
[16] M. Balasubramanian, X. Sun, X.Q. Yang, J. McBreen, J. Electrochem. Soc. 147 (2000 2903).
[17] I. Nakai, T. Nakagome, Electrochem, Solid State Lett. 1 (1998) 259.
[18] J. Rodríguez-Carvajal, Fullprof-3. 6 Program for Reitveld Refinement (2006).
[19] S. Kraft, J. Stümpel, P. Becker, U. Kuetgens, Rev. Sci. Instrum. 67 (1996) 681.
[20] M. Balasubramanian, X. Sun, X.Q. Yang, J. McBreen, J. Power Sources 92 (2001) 1.
[21] Z.H. Lu, L.Y. Beaulieu, R.A. Donaberger, C.L. Thomas, J.R. Dahn, J. Electrochem. Soc. 149 (2002) A778.
[22] S.H. Kang, S.H. Park, C.S. Johnson, K. Amine, J. Electrochem. Soc. 154 (2007) A268.
[23] J.R. Mueller-Neuhaus, R.A. Dunlap, J.R. Dahn, J. Electrochem. Soc. 147 (2000) 3598.
[24] S.H. Kang, W.S. Yoon, K.W. Nam, X.Q. Yang, D.P. Abraham, J. Mater. Sci. 43 (2008) 4701.
[25] M. Balasubramanian, J. McBreen, I.J. Davidson, P.S. Whitfield, I. Kargina, J. Electrochem. Soc. 149 (2002) A176.
[26] A.J. Davenport, H.S. Isaäcs, G.S. Frankel, A.G. Schrott, C.V. Jahnes, M.A. Russak, J. Electrochem. Soc. 138 (1991) 338.
[27] A. Manceau, L. Charlet, J. Colloid Interface Sci. 148 (1992) 425.
[28] W.E. O'Grady, K.I. Pandya, K.E. Swider, D.A. Corrigan, J. Electrochem. Soc. 143 (1996) 1613.
[29] W.S. Yoon, M. Balasubramanian, K.Y. Chung, X.Q. Yang, J. McBreen, C.P. Grey, D.A. Fischer, J. Am. Chem. Soc. 127 (2005) 17479.